Practical Modeling for Wind Load Paths in a Realistic Light-Frame Wood House

Kathryn S. Pfretzschner[1]; Rakesh Gupta, M.ASCE[2]; and Thomas H. Miller, M.ASCE[3]

Abstract: The objective of this study was to develop and validate practical modeling methods for investigating load paths and system behavior in a realistic light-frame wood structure. The modeling methods were validated against full-scale tests on subassemblies and an L-shaped house. The model of the L-shaped house was then modified and used to investigate the effects of reentrant corners, wall openings, and gable-end retrofits on system behavior and load paths. Results showed that the effects of adding reentrant corners and wall openings on uplift load distributions were dependent on the orientation of the trusses with respect to the walls. Openings added to walls parallel to the trusses have the least effect on loads carried by the remaining walls in the building. Varying reentrant corner dimensions under design wind loads caused increasing degrees of torsion throughout the house depending on the relative location and stiffness of the in-plane walls (parallel to the wind loads) and the assumed direction of the wind loads. Balancing the stiffness of the walls on either side of the house with the largest reentrant corner helped to decrease torsion in the structure under lateral loads. Finally, although previous full-scale tests on gable-end sections verified the effectiveness of the gable-end retrofit that was recently adopted into recent Florida building code, questions remained about the effects of the retrofit on torsion in a full building. The current study found that adding the gable-end retrofits to the L-shaped house did not cause additional torsion. **DOI: 10.1061/(ASCE)CF.1943-5509.0000448.**

Author keywords: System behavior; Reentrant corners; Wall openings; Gable-end retrofits.

Introduction

In the United States, wind damage accounted for approximately 70% of insured losses between 1970 and 1999 (Holmes 2001). Wood-frame residential structures are particularly vulnerable to damage from wind because of their light weight. Additionally, most existing single-family houses in the United States were constructed before building codes were updated after Hurricane Andrew in 1992. More recent wind storms in the United States, including the 2005 Hurricane Katrina and the 2011 Joplin, Missouri, and Tuscaloosa, Alabama, tornadoes, have shown that structural damage from wind is still a prevalent issue, especially for wood-framed residential structures. Structural investigations from these hurricane and tornado events showed that the main source of damage in houses was an overall lack of design for uplift load paths (van de Lindt et al. 2007; Prevatt et al. 2012). Additionally, gable-end failures were reported as an area of concern (van de Lindt et al. 2007; Prevatt et al. 2012). To develop retrofitting options and improve building codes for residential structures, it is necessary to gain a better understanding of system behavior and load paths in light-frame structures.

Analyzing system behavior in complex structures requires the development of practical and accurate analytical models validated against full-scale tests. Phillips et al. (1993) and Paevere et al. (2003) performed full-scale tests on realistic, rectangular, and L-shaped residential structures. Results from these studies showed that light-frame roof diaphragms act relatively stiff compared with shear walls. Additionally, in-plane walls (parallel to applied lateral loads) are capable of sharing approximately 20–80% of their loads with other walls in the structure depending on the relative location and stiffness of the surrounding walls (Paevere et al. 2003). Data from these tests have also been used by a number of researchers to develop practical models for load path analysis.

Doudak (2005) developed a nonlinear model of the Paevere et al. (2003) house using a rigid element for the roof diaphragm. Individual sheathing nail connections were modeled using nonlinear spring elements. The model was capable of predicting lateral load distributions to the walls; however, the level of detailing in the walls proved time consuming. Kasal (1992) and Collins et al. (2005) developed nonlinear models of the Phillips et al. (1993) and Paevere et al. (2003) houses, respectively, also using rigid elements for the roof diaphragm. Unlike Doudak (2005), the in-plane stiffness of the shear walls was controlled using diagonal nonlinear springs. This reduced the amount of time required for modeling; however, full-scale tests were necessary to determine the nonlinear stiffness of the springs and material properties for the structure. None of these models were used to examine uplift load paths. Shivarudrappa and Nielson (2011) modeled uplift load paths in light-frame roof systems. For increased accuracy, the models incorporated individual trusses, sheets of sheathing (modeled with individual nail connections), and semirigid roof-to-wall connections. Results from the model showed that load distribution was affected by the location of gaps in the sheathing and the stiffness of the sheathing and connections.

Martin et al. (2011) developed a simple linear model of a rectangular structure tested at one-third scale at the University of Florida. The model relied on material properties and wall stiffness properties readily available in industry standards. The in-plane stiffness of the walls was controlled by adjusting the shear modulus of the wall sheathing. The roof diaphragm was modeled as

[1]Former Graduate Research Assistant, Dept. of Wood Science and Engineering and School of Civil and Construction Engineering, Oregon State Univ., Corvallis, OR 97331. E-mail: Kathryn.Pfretzschner@kpff.com

[2]Professor, Dept. of Wood Science and Engineering, Oregon State Univ., Corvallis, OR 97331 (corresponding author). E-mail: rakesh.gupta@oregonstate.edu

[3]Associate Professor, School of Civil and Construction Engineering, Oregon State Univ., Corvallis, OR 97331.

Note. This manuscript was submitted on September 18, 2012; approved on February 25, 2013; published online on February 27, 2013. Discussion period open until November 1, 2014; separate discussions must be submitted for individual papers. This paper is part of the ***Journal of Performance of Constructed Facilities***, Vol. 28, No. 3, June 1, 2014. ©ASCE, ISSN 0887-3828/2014/3-430–439/$25.00.

semirigid with individual trusses and sheathing, although gaps between individual sheets of sheathing were not included. Martin et al. (2011) found that the linear modeling methods were sufficient for predicting lateral load paths and uplift load paths through the structure when loaded within the elastic range. Additionally, the distribution of uplift loads was highly dependent on the orientation of the roof trusses. The modeling methods developed by Martin et al. (2011) were used in the current study to analyze lateral and uplift load paths in a more realistic light-frame house. A more detailed review of previous full-scale testing and modeling can be found in Pfretzschner (2012).

Research Methods

The two main objectives of this study were to further develop and validate the practical, linear modeling methods of Martin et al. (2011) for a rectangular building and to apply the modeling methods toward investigating uplift and lateral load paths in a realistic light-frame structure with complex geometry (L-shaped house). The modeling methods were developed using *SAP2000* software (Computers and Structures 2009). Additional details about the research methods can be found in Pfretzschner (2012).

Modeling Methods

Framing Members

Framing members, including wall studs and truss chords, were modeled using the frame element of the *SAP2000* software. The frame element was assigned the actual cross section of each framing member. Multiple framing members located side by side, such as a double stud or double top plate, were modeled using a single frame element with a cross section equal to the sum of the individual cross sections of the framing members.

Isotropic material properties for the framing members were determined using longitudinal design properties listed in the *National Design Specification for Wood Construction* (NDS) of the American Forest & Paper Association [AF&PA (2005a)] based on wood species and grade. Adjustment factors for moisture content, incising, and so forth were applied to the design properties as specified by the NDS (AF&PA 2005a).

Sheathing

Wall sheathing was modeled using the layered shell element of the *SAP2000* software with plywood and gypsum wallboard (GWB) assigned as individual layers. Each shell element was modeled through the center of the wall studs with the sheathing layers displaced to either side of the wall. Roof and ceiling sheathing were also represented using the layered shell element modeled through the centerline of the truss chords with one layer of either plywood or GWB displaced accordingly.

Plywood layers were assigned orthotropic properties calculated using *OSULaminates* software (Nairn 2007). Plywood sheathing layers for the walls and roof were assigned in-plane and out-of-plane properties, respectively, based on their general behavior within the full building. GWB layers were assigned isotropic material properties listed by the Gypsum Association (2010).

In accordance with Martin et al. (2011), individual sheets of plywood and GWB were not modeled as separate elements. Instead, one continuous shell element was applied to each wall, ceiling, and roof surface and meshed into smaller elements for analysis. Although the effects of gaps between individual sheathing members were neglected, validation studies against full-scale tests showed that these methods were sufficient for portraying system behavior and load distribution.

Framing Connectivity

All framing connections were modeled as either simple pinned or rigid connections. Trusses were modeled with pinned connections at the ends of the webs and at the ridge. Rigid connections were used at the truss heels, and top and bottom chords were modeled as continuous members through the web connections. Truss-to-wall connections were modeled as rigid connections and were not coincident with the heel connections (Martin et al. 2011); however, in retrospect, they would be more accurately modeled as pins and rollers. Gable-end trusses were also rigidly connected to the gable-end walls.

All framing connections in the walls were modeled as pinned connections. This allowed for the stiffness of the walls to be controlled entirely by the sheathing properties. Shear wall stiffness is highly dependent on the spacing of the nail connections between the sheathing and framing members. As in Martin et al. (2011), the effects of edge nail spacing on wall stiffness were incorporated by adjusting the shear modulus, G_{12}, of the wall sheathing.

Sheathing G_{12} Adjustment Procedure

To account for the effects of sheathing edge nail spacing, the shear modulus, G_{12} of the sheathing was adjusted using a procedure similar to the correlation procedure used by Martin et al. (2011). The shear modulus of the sheathing was adjusted to account for the effects of edge nail spacing on overall wall stiffness rather than modeling individual nailed connections. The procedure in the current study was performed using a simple *calibration model* of a wall in *SAP2000* with a specific length, rigid supports, no openings, and sheathed on one side only. Material properties were assigned to the sheathing using the previously described methods. G_{12} of the sheathing was then altered until the deflection of the calibration model matched the predicted deflection calculated using Eq. C4.3.2-2 from AF&PA (2005b) for a specific edge nail spacing and wall length.

Eq. C4.3.2-2 is a three-term, linear equation used to predict deflections of wood-framed shear walls based on "framing bending deflection, panel shear deflection, deflection from nail slip, and deflection due to tie-down slip" (AF&PA 2005b). The effects of panel shear and nail slip are incorporated into an apparent stiffness term, G_a. Values for G_a are tabulated in AF&PA (2005b) based on sheathing material, framing layout, and edge-nail spacing. Because rigid supports were used in the calibration model, the deflection caused by tie-down slip was ignored in the three-term equation. The purpose of the calibration model was to determine the required stiffness of the sheathing element. The effects of the anchor bolts and hold-downs were incorporated later on into the actual wall models used in the shear wall validation and full building models by using linear springs with realistic stiffness properties.

Repeating this method for shear walls of various lengths revealed that the required G_{12} for a specific edge nail spacing varied approximately linearly with wall length. Therefore, for a building with multiple wall lengths and uniform edge nail spacing, this procedure is only necessary for the shortest and longest walls in the building. Additionally, G_{12} for the plywood sheathing and GWB sheathing can be determined separately using the previously mentioned procedure for a wall sheathed on one side and applied to the respective sides of a wall sheathed on two sides. This method is supported by Patton-Mallory et al. (1984), who found that the stiffness of a wall sheathed on two sides is equal to the sum of the stiffness of two walls sheathed on one side with the same materials.

Application of the sheathing adjustment procedure to the Paevere et al. (2003) house is shown in the following model validation procedure section.

J. Perform. Constr. Facil., 2014, 28(3): 430-439

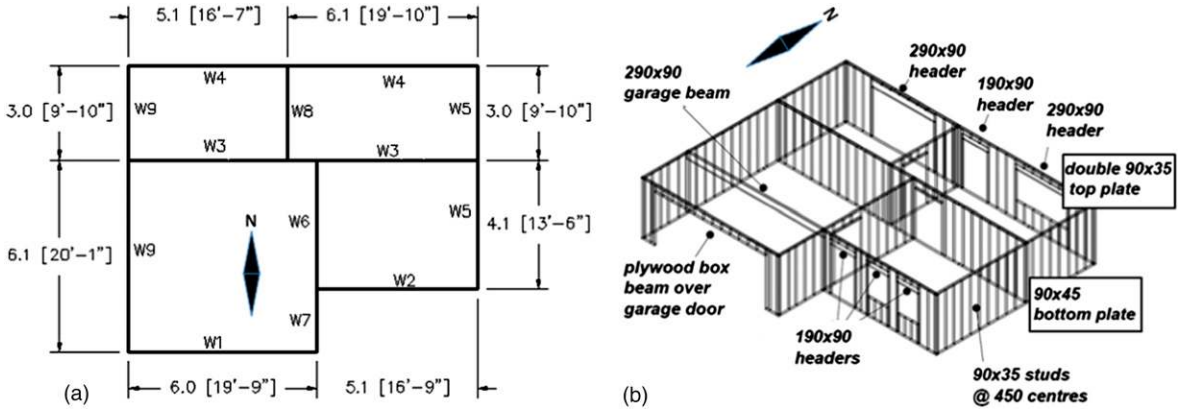

Fig. 1. (a) Floor plan with centerline dimensions [m (ft-in.)] and wall designation; (b) wall framing (mm)

Wall Anchorage

Anchor bolts and hold-downs were modeled using directional linear spring elements. Three springs were used for the anchor bolts: one oriented in the vertical Z-direction (representing the axial stiffness of each bolt connection) and two oriented in the lateral X-direction and Y-direction (representing the shear stiffness of each bolt connection). Hold-down devices were represented with only one spring oriented in the Z-direction.

The axial stiffness of the anchor bolts was assigned in accordance with Martin et al. (2011) based on full-scale tests performed by Seaders (2004). The full-scale tests incorporated the effects of bolt slip and wood crushing under the washers. The lateral stiffness of the anchor bolts was calculated using equations for the load slip modulus, γ, for dowel-type connections in Section 10.3.6 of the NDS (AF&PA 2005a). Finally, the axial stiffness of the hold-down devices was determined from properties published by the manufacturer Simpson Strong-Tie (Simpson Strong-Tie 2014).

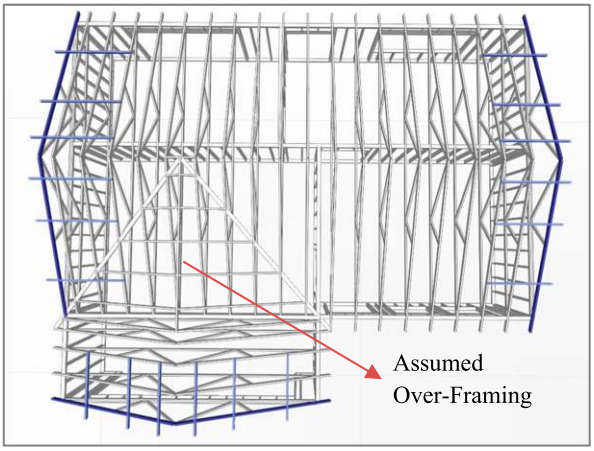

Fig. 2. Truss orientation and gable-end framing

Model Validation Procedure

Similar to Martin et al. (2011), the modeling methods in this study were validated against full-scale tests. Subassembly models, including two-dimensional trusses, three-dimensional roof assemblies, and two-dimensional shear walls, were validated against tests performed by Wolfe et al. (1986), Wolfe and McCarthy (1989), and Dolan and Johnson (1996), respectively. Shear walls from Dolan and Johnson (1996) were anchored with both anchor bolts and hold-downs allowing for the simultaneous validation of anchorage and shear wall modeling methods. Details for the subassembly models are included in Pfretzschner (2012). The final validation study was performed using full-scale tests on a realistic L-shaped house from Paevere et al. (2003).

Paevere et al. (2003) performed static, cyclic, and destructive load tests on a full-scale, L-shaped house (Fig. 1). The house was designed to reflect a typical North American stick-frame house with a gable-style roof. Construction details for the L-shaped house can be found in Paevere et al. (2003) and Paevere (2002). Results from the static load tests were used to validate a model of the house.

Fig. 1 shows the layout and framing used for the walls in the house, including six exterior shear walls (W1, W2, W4, W5, W7, and W9) and three interior nonload bearing walls (W3, W6, and W8). The exterior walls were 2.4 m (7.9 ft) tall. The interior walls were modeled 25 mm (1 in.) shorter than the exterior walls; therefore, the trusses spanned the exterior walls only (P. Paevere, personal communication, 2012). Wall W3 was connected to the trusses using nonstructural slip connections to restrain the trusses laterally (Paevere 2002). These connections were modeled in *SAP2000* using two-joint link elements fixed in the direction parallel to the wall. Interior Walls 6 and 8 were not connected to the trusses.

The gable roof was modeled as a semirigid diaphragm with 1.6-m-tall (5.2-ft-tall) Fink trusses spaced 0.6 m (2 ft) on center and oriented as shown in Fig. 2 and plywood sheathing. Unsheathed Fink trusses were also used for the gable-end trusses. Framing members used for the truss chords and webs were 35×90 mm (1.4×3.5 in.) and 35×70 mm (1.4×2.8 in.), respectively. Details for the roof overframing where the two legs of the L meet above the garage were not included in Paevere (2002) or Paevere et al. (2003). Therefore, overframing in the model was assumed based on typical North-American residential construction methods shown in Fig. 2. It was modeled as a ridge board with rafters. All framing members were assigned the same cross-sectional dimensions as the roof truss chords. All connections were modeled as pinned.

All framing members in the house were Australian radiata pine sawn lumber. Because radiata pine is not included in AF&PA (2005a), the modulus of elasticity reported by Paevere (2002) of 10,000 MPa (1,450 ksi) was used for the frame elements in *SAP2000*. Sheathing consisted of 9.5-mm-thick (0.375 in.-thick) and 12.5-mm-thick (0.492-in.-thick) plywood on the walls and roof, respectively, with 13-mm-thick (0.5-in.-thick) GWB interior lining on the walls and ceiling. All walls were fully sheathed on the interior

with GWB. Exterior walls were fully sheathed on the outside with plywood with the exception of Walls 5 and 9. The partial exterior sheathing used for Walls 5 and 9 is shown in Fig. 3.

Table 1 provides the material properties used to model the sheathing elements. Fig. 4 shows the required G_{12} versus wall length for the plywood and GWB wall sheathing based on edge fastener spacing. The fasteners used for the plywood sheathing were equivalent to 6d common nails spaced at 152 mm (6 in.) along the edges. The GWB fasteners were equivalent to No. 6 drywall screws spaced 305 mm (12 in.) along the edges. The maximum fastener spacing listed in AF&PA (2005b) of 203 mm (8 in.) for GWB sheathing was used to determine values of G_{12} for the GWB in the model.

The walls were anchored with 12.7-mm-diameter (0.5-in.-diameter) anchor bolts only (no hold-downs were used). Vertical and lateral springs used to represent the axial and shear behavior of the bolt connections were assigned a stiffness of 6.1 kN/mm (35 kip/in.) and 16.7 kN/mm (95.5 kips/in.), respectively. Stiffness properties were determined from Seaders (2004) and AF&PA (2005a) as explained in the modeling methods. Each anchor bolt in the full-scale house was connected to a load cell capable of measuring lateral and vertical reactions. Reactions at the anchor bolts in the model were validated against reactions from Paevere et al. (2003) for 15 static load tests consisting of one gravity load test and 14 lateral concentrated load tests. Table 2 lists the material densities used to model the self-weight (gravity loads) of the house. A complete list of lateral load cases can be found in either Paevere (2002) or Pfretzschner (2012).

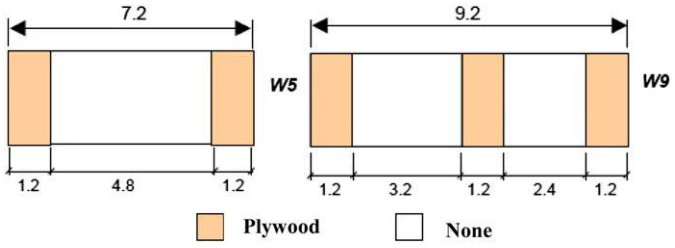

Fig. 3. Plywood sheathing on exterior of Walls 5 and 9

Load Path Investigations

After the modeling methods were validated, variations of the Paevere et al. (2003) house were created and used to perform load path investigations for uniform uplift pressures and ASCE/SEI 7-05 (ASCE 2005) design wind loads. All structures used in the investigations were modeled based on the materials and construction methods used by Paevere et al. (2003) with the following exceptions. (1) Gable-end overhang framing was changed to out-looker or outrigger style framing commonly used in North America (Martin et al. 2011). (2) Gable-end trusses were changed from Fink trusses to more common, nonstructural gable-end trusses. Modified gable-end framing is shown in Fig. 5. (3) The exterior was fully sheathed with plywood, including the gable-end trusses. The shell element used to model the sheathing on the gable-end truss was not connected to the shell element used for sheathing on the gable-end wall. (4) Simpson Strong-Tie (Pleasanton, California) HDU2 hold-downs, modeled with an axial stiffness of 6.1 kN/mm (35 kip/in.), were added to the exterior walls at the ends and at either side of the door openings.

For each load path investigation, index buildings were created as a baseline for load path comparisons. The index buildings were then altered systematically to analyze the effects of geometric variations (wall openings and reentrant corners) and gable-end retrofits on uplift and lateral load paths. Detailed descriptions of the structures

Table 1. Sheathing Material Properties

Material	Properties	Source
Plywood sheathing (roof)	E_1 = 8,280 MPa (1,201 ksi)	*OSULaminates* (Nairn 2007) (flexural properties)
	E_2 = 2,393 MPa (347 ksi)	
	U_{12} = 0.011	
	G_{12} = 482 MPa (70 ksi)	
Plywood sheathing (walls)	E_1 = 7,017 MPa (1,018 ksi)	*OSULaminates* (Nairn 2007) (in-plane properties)
	E_2 = 3,657 MPa (530 ksi)	
	U_{12} = 0.016	
GWB (walls and ceiling)	E_1 = 1,820 MPa (264 ksi)	Gypsum Association (2010)
	E_1 = 1,820 MPa (264 ksi)	
	U_{12} = 0.3	

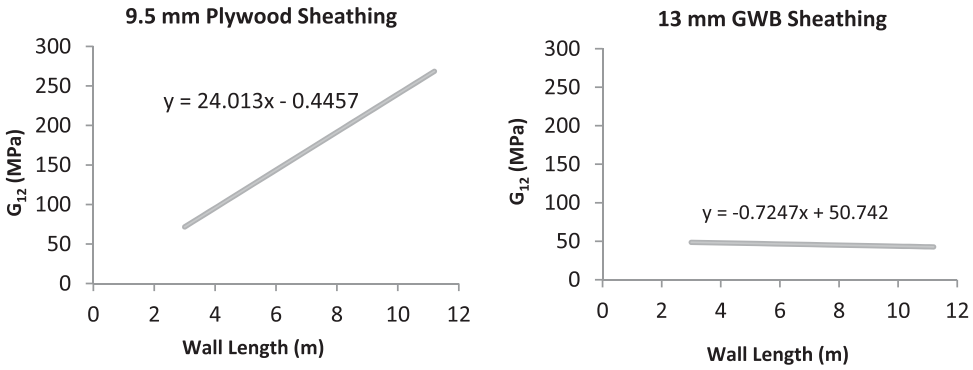

Fig. 4. G_{12} versus wall length for plywood and GWB wall sheathing

J. Perform. Constr. Facil., 2014, 28(3): 430-439

used in the load path investigations can be found in Pfretzschner (2012).

Uniform Uplift Investigation

As an extension of Martin et al. (2011), the effects of reentrant corners and large wall openings were explored under a uniform uplift pressure of 2.4 kPa (50 psf) acting normal to the surface of the roof.

Two simple index buildings were used for the uplift investigation: a rectangular index building and an L-shaped index building. The L-shaped index building had the same plan geometry as the Paevere et al. (2003) house with the modifications described previously (no interior walls, no wall openings, and no GWB lining). The rectangular index building was then created by removing the short leg of the L and extending Wall 2. The wall designations used by Paevere et al. (2003) (Fig. 1) were maintained throughout both load path investigations. Similar to Martin et al. (2011), the self-weight of the buildings was not included to analyze load paths caused by uplift pressures only. Reactions at the anchor bolts and hold-downs of the L-shaped index building were compared with the rectangular building to analyze the effects of the reentrant corner.

The redistribution of load paths caused by large wall openings was also explored in this investigation. Martin et al. (2011) analyzed the effects of wall openings on uplift load paths in a simple rectangular building. In the current study, the effects of large 3.2-m-long (10.5 ft-long) wall openings in the L-shaped index building were explored. Wall openings were added to the building one at a time in the following locations, representing scenarios that were not previously explored by Martin et al. (2011): Wall 2 adjacent to the reentrant corner, Wall 4 opposite the reentrant corner, Wall 9 centered under the gable end, and Wall 9 opposite the reentrant corner. Because of the configuration of the roof, Wall 9 represents both a gable-end wall and a side wall with trusses running both parallel and perpendicular to the wall.

Table 2. Material Densities Used for Building Self-Weight

Material	Density, kg/m^3 (pcf)	Source
Framing members	550 (34.3)	Paevere (2002)
Plywood	600 (37.5)	Engineered Wood Products Association of Australia (2009)
GWB	772 (48.2)	Gypsum Association (2010)

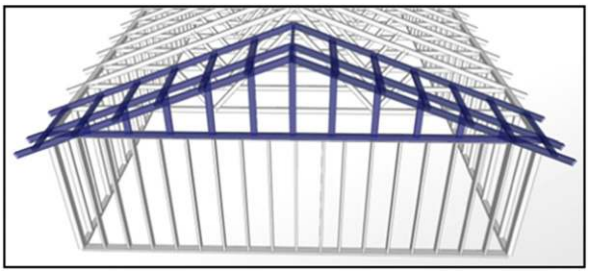

Fig. 5. Modified gable-end framing for load path investigations

Wind Load Investigation

The second load path investigation explored load paths in a more realistic house with applied ASCE/SEI 7-05 design wind loads. Design loads were calculated using the main wind force resisting system (MWFRS) method 2 (ASCE 2005). Although ASCE/SEI 7-05 MWFRS codified pressures are intended for buildings with regular plan geometry, a method for adapting the pressures to buildings with reentrant corners is given in Mehta and Coulbourne (2010). This methodology was adopted for the current study. Additional methods of determining design wind loads for irregular buildings are discussed in Pfretzschner (2012).

Three wind directions were considered with design loads calculated based on ASCE/SEI 7-05 (ASCE 2005) Load Cases 1 and 3 as shown in Fig. 6. Load Case 1 includes all windward, leeward, sidewall, and roof parallel to wind pressures indicated by Fig. 6-6 of ASCE/SEI 7-05. Load Case 3 is meant to simulate diagonal winds by combining leeward and windward pressures for X and Y winds acting simultaneously at 75% of their full design value (Mehta and Coulbourne 2010). Parameters for the design wind loads were selected in accordance with Martin et al. (2011), including a basic wind speed of 209 km/h (130 mi/h), a topographic factor, K_{zt}, of 1.0, and exposure category, B. The building was assumed to be a low-rise enclosed building with occupancy Category II and an importance factor of 1.0. Positive internal pressure was used to produce worst-case uplift scenarios.

The index structure for this investigation was a realistic L-shaped index house, different from the L-shaped index building, representing the Paevere et al. (2003) house with the gable-end framing, sheathing, and hold-down modifications described previously. The L-shaped index house was then altered to investigate the effects of (1) the addition of gable-end retrofits at every gable-end stud and (2) the effects of increasing the size of the reentrant corner. The gable-end retrofits were modeled based on the C-shaped, gable-end retrofit recently adopted into the 2010 Florida building code [International Code Council (ICC) 2011]. An additional stud was added at each vertical web in the gable-end trusses, with the strong axis oriented perpendicular to the wall (forming an L) to reinforce the webs against out-of-plane winds. The ICC (2011) actually only requires the gable-end retrofits at studs exceeding 0.9144 m (3 ft) in length. However,

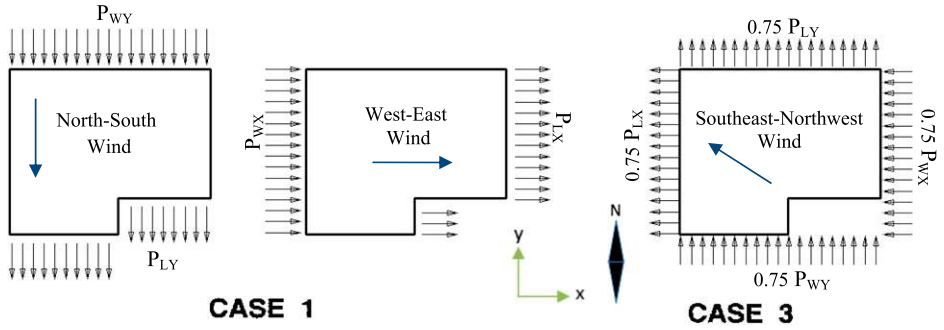

Fig. 6. Wind directions and ASCE/SEI 7-05 (ASCE 2005) load cases

J. Perform. Constr. Facil., 2014, 28(3): 430-439

the purpose in adding the retrofits was to examine any torsion in the building and not the effectiveness of the retrofit itself. The study shows that even with retrofits at every stud there is no additional torsion in the building. Additionally, horizontal braces were added to help the transfer load from the gable-end wall into the roof and ceiling diaphragm. Additional details about the retrofit can be found in the ICC (2011). Fig. 7 shows one of the C-shaped retrofits in the model added at every gable-end stud. Connections between the retrofit studs and horizontal braces were accomplished with steel L-straps and compression blocks and assumed to be rigidly connected in the model because of the overall configuration of the connection. No physical testing results are available; therefore, it is possible that a pinned connection is more appropriate.

The effects of the reentrant corner were explored by altering the short leg of the L-shaped index house to create three different sized reentrant corners: small, medium, and large. For the small and medium reentrant corners, the leg was shortened and lengthened by 2.4 m (7.9 ft). The large reentrant corner was created by extending the leg so that the dimensions of the reentrant corner had a 1:1 ratio. Wind loads for the reentrant corner variations were adjusted accordingly based on the dimensions of the house.

Results and Discussion

Model Validation

Subassemblies

Subassembly models were used to validate the applicability of previously described modeling methods in predicting two-dimensional (2D) and three-dimensional (3D) system behavior. The 2D models of individual trusses validated the use of ideal pinned and rigid connections between truss chords and webs. The 3D models of roof assemblies validated the use of the layered shell element for modeling plywood sheathing. The roof assembly models were capable of predicting load sharing and relative truss deflection in roofs with variable truss stiffness. Finally, models of the 2D shear walls validated methods for incorporating the effects of sheathing edge-nail spacing, wall openings, and wall anchorage on shear wall stiffness. Full details and results for the subassembly validation studies are included in Pfretzschner (2012).

Paevere et al. (2003) House

The full-scale L-shaped house, tested by Paevere et al. (2003), was used to validate the ability of the model to predict load sharing between walls connected by the roof diaphragm in a realistic house. Reactions at the anchor bolts in the model were compared against reactions in the full-scale house for 15 static load cases. The load distributions here and for full building models are examined at the foundation level rather than at the roof-to-wall connections. The variation may be less at the foundation level as the loads distribute through the walls. The first static load case included gravity loads only to determine the self-weight of the house. Paevere et al. (2003) measured a self-weight of 50.8 kN (11.4 kips), which was only 9% smaller than the self-weight of the model [55.7 kN (12.5 kips)], and this was considered to be close enough.

The remaining 14 load cases consisted of concentrated lateral loads applied at various locations along the top chords of Walls 4 and 5 and at various angles at the roof ridge directly above Wall 5. The distribution of the lateral loads to the in-plane walls of the model was compared with reactions from Paevere et al. (2003). Fig. 8, for example, compares the load distributions from the test house and the model for load Case 4. Results from all 14 lateral load cases can be found in Pfretzschner (2012). Overall, the model proved capable of predicting the overall trends in load distributions (Fig. 8) to the in-plane walls. Reactions at the walls carrying the maximum in-plane load were predicted within 20% error on average. For example, the largest load in Fig. 8 occurred at Wall 3 and was accurate to about 17%. This is similar to the level of accuracy reported by Doudak (2005) for static loading and elastic behavior of the structure.

Uniform Uplift Investigation

The vertical reactions and changes in reaction at the anchor bolts and hold-downs of the models used in the uplift investigation were recorded and plotted in bubble plots. Each bubble represented an anchor bolt or hold-down, whereas the size of the bubble represented the magnitude of either the uplift reaction or change in reaction at that anchorage device. The locations of the hold-downs were designated with a multiplication symbol. Detailed reaction plots for all model variations can be found in Pfretzschner (2012).

Rectangular versus L-Shaped Buildings

To analyze the effects of reentrant corners, the uplift reactions for the rectangular and L-shaped index buildings were plotted in Fig. 9. Uplift reactions in the rectangular building were symmetrical with a maximum reaction of 11.0 kN (2.5 kips), which is 0.17 kN/m^2 of floor area, and occurring at the anchor bolts at the center of the side walls (Walls 2 and 4). Because the roof trusses spanned between the side walls, most of the load applied to the roof was directed into the side walls rather than the gable-end walls. The maximum uplift reaction in the L-shaped index building, on the other hand, was 14.7 kN (3.3 kips), which is 0.16 kN/m^2 of floor area, and occurring at the

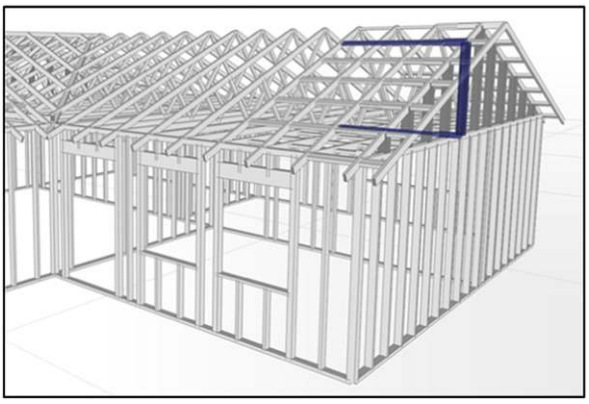

Fig. 7. Example of C-shaped gable-end retrofit at gable-end stud

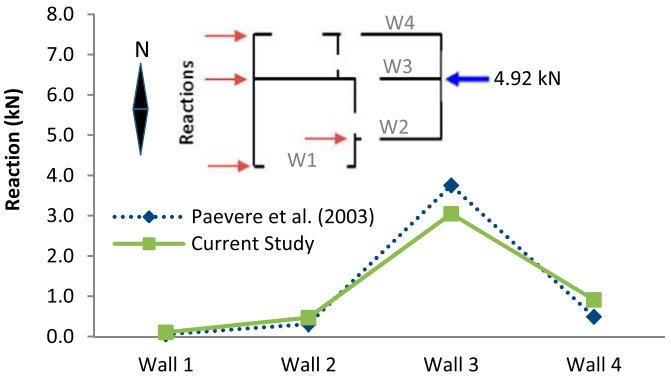

Fig. 8. Load distribution plot for Paevere et al. (2003) load Case 4

J. Perform. Constr. Facil., 2014, 28(3): 430-439

hold-down directly under the reentrant corner. In this case, the uplift loads that would have been transferred to the west side of Wall 2 in the rectangular building were instead transferred to the garage beam in the L-shaped building [Fig. 1(b)]. The garage beam then directed the loads to the reentrant corner and Wall 9 opposite the reentrant corner, causing load concentrations at these locations. Uplift load concentrations also occurred at anchor bolts under Wall 4, directly opposite the reentrant corner. The flow of loads in the L-shaped index building is illustrated by the arrows in Fig. 9. Trusses span perpendicularly from the reentrant corner to Wall 4 at this location. The load distribution to Wall 5, parallel to the trusses, was not affected by the addition of the reentrant corner. This suggests that the redistribution of uplift loads caused by a reentrant corner is dependent on the orientation of the roof trusses with respect to the walls. A similar observation was noted by Martin et al. (2011) when investigating the effects of wall openings. Future research should examine the effects of reentrant corners in buildings with different truss orientations.

Effects of Wall Openings

Martin et al. (2011) explored the effects of large wall openings placed in the gable-end walls and side walls of a rectangular building under uniform uplift pressure. The current study examined openings in an L-shaped building with a reentrant corner and trusses oriented in two orthogonal directions. Similar to Martin et al. (2011), the opening centered under the gable-end portion (north end) of Wall 9 caused relatively localized effects, increasing uplift loads in the side wall portion (south end) of Wall 9 and having negligible effects on walls on the opposite side of the building. The openings placed in the side walls, on the other hand, had more global effects on uplift reactions throughout the building. Fig. 10 shows the change in uplift reactions caused by openings in the two different side walls: Wall 4 (opposite the reentrant corner) and Wall 2 (adjacent to the reentrant corner). The increase of 60% in Fig. 10 is compared with the uplift reaction at the same location along Wall 2 in the L-shaped index building without wall openings in Fig. 9 (not labeled). As expected, uplift loads at the location of the openings were redirected through the headers to either side of the doors causing load concentrations at the hold-downs directly under the door jams. The largest load concentrations were seen on the side of the opening in Wall 2, closest to the reentrant corner. Uplift reactions at this point increased by 60% over the reactions seen in the building without openings. Comparatively, the opening in Wall 4 caused less than a 30% increase in uplift loads at either side of the opening. The larger load concentration at the opening in Wall 2 was likely caused by the uplift load concentrations in Wall 2 from the reentrant corner itself.

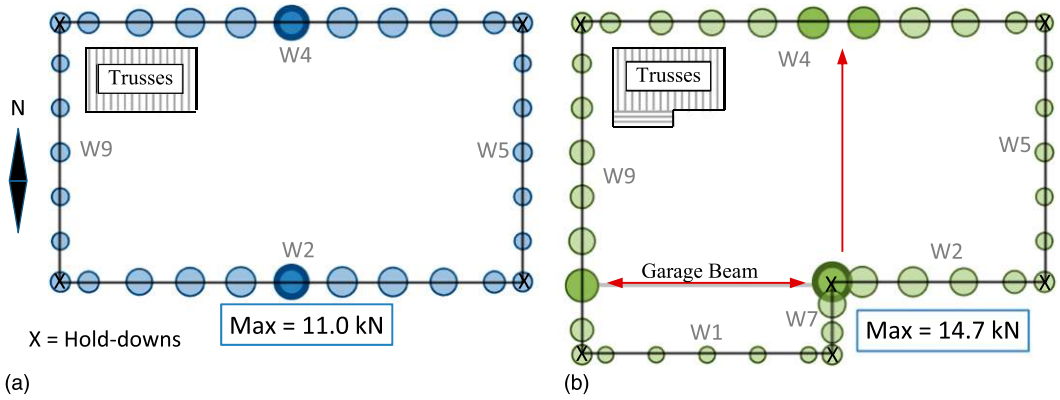

Fig. 9. Uplift reactions at wall supports: (a) rectangular; (b) L-shaped index buildings under uniform uplift pressure of 2.4 kpa (50 psf)

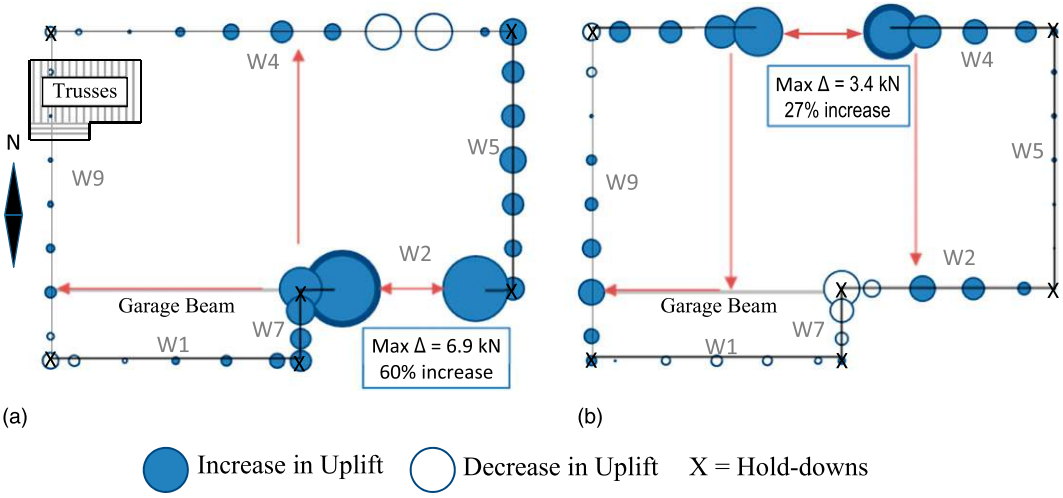

Fig. 10. Change in uplift reactions (magnified four times) caused by openings in (a) Wall 2 and (b) Wall 4 under uniform uplift; arrows represent load paths

J. Perform. Constr. Facil., 2014, 28(3): 430-439

As in Martin et al. (2011), openings placed in the side walls in this investigation also caused uplift load concentrations in the remaining side walls. Examining the truss orientation in the building shows that uplift loads at these points of concentration were clearly transferred from either side of the wall opening by the roof trusses. In the case of the opening in Wall 4, for example, uplift loads were transferred from the east side of the wall opening, through the north-south trusses, to the opposite side wall (Wall 2). Uplift loads were also transferred from the west side of the opening through the north-south trusses to the garage beam shown in Fig. 1(b), and they were redirected through the garage beam and the east-west trusses to Wall 9 (adjacent to Wall 4). Similar system behavior was seen for the opening in Wall 2 as shown in Fig. 10 and for other side wall openings included in Pfretzschner (2012). This strongly supports findings from Martin et al. (2011) that the effects of openings on uplift load distribution are dependent on the relative truss orientation with respect to the walls. The effects of openings in walls perpendicular to the trusses were shared by other walls in the building spanned by the same trusses, whereas the effects of openings in walls parallel to the trusses were more isolated.

Finally, Martin et al. (2011) reported that the addition of an opening to any wall resulted in a decrease in the total load carried by the wall. In the current study, the opening in Wall 2 also caused a decrease in the total load carried by the wall of up to 20%. The opening placed in Wall 4, however, caused a 0.2% increase in the amount of total uplift load carried by the wall. It is likely that this small increase was caused by the effects of the reentrant corner.

Wind Load Investigation

Uplift reactions for each of the model variations in the wind load investigation were also plotted in bubble graphs and included in Pfretzschner (2012). Fig. 11 shows the uplift reactions at the anchor bolts and hold-downs in the L-shaped index house for each wind load case. In all cases, uplift load concentrations were seen at the hold-downs located under the corners of the house and on either side of the door openings. In addition, to determine whether the large uplift reactions at the west gable end were caused by the geometry of the building or the selected load cases, a fourth load case for east-to-west (E-W) winds was added. This demonstrated that uplift reactions at the east gable end under the E-W wind loads were of similar magnitude to the reactions at the west gable end under west-to-east (W-E) wind loads.

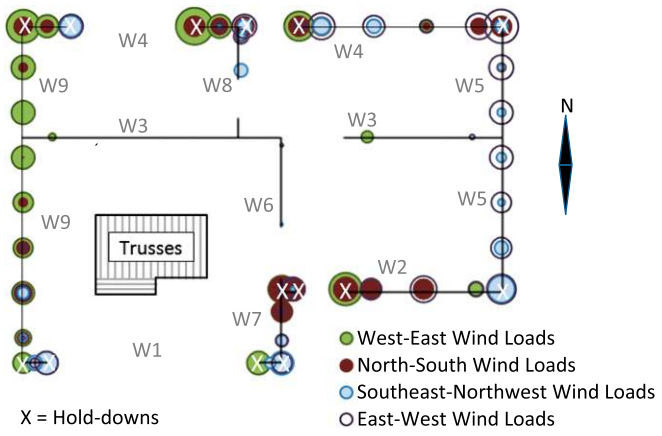

Fig. 11. Uplift reactions in L-shaped index house under ASCE/SEI 7-05(ASCE 2005) design wind loads

Lateral load distributions to the walls parallel to the wind loads for each model were also plotted (Fig. 12) and used to support the findings subsequently described. For the southeast-northwest load case, lateral load distributions to both the north-to-south (N-S) and E-W walls were plotted. Walls 6–8 (shown individually in Fig. 1) were grouped together here to simplify data presentation.

Addition of Gable-End Retrofits

Because of the number of gable-end failures seen in the aftermath of hurricanes, the 2010 Florida building code recently adopted a C-shaped gable-end retrofit for existing buildings (ICC 2011). Full-scale tests performed on gable-end sections (comprised of four Fink trusses and a gable-end wall) by Suksawang and Mirmiran (2009) showed that the retrofit sufficiently increased the strength of the gable ends. However, questions remained about whether load redistribution caused by the retrofit could cause additional torsion within a full building (beyond the original design). To address this question, C-shaped retrofits were modeled at every gable-end stud within the L-shaped index house used in this investigation.

The distribution of lateral loads and top plate deflections of the walls were then analyzed under ASCE/SEI 7-05 (ASCE 2005) design wind loads for signs of torsion. For all wind load cases, the addition of the gable-end retrofits to the L-shaped index house caused negligible changes in lateral reactions under the walls parallel to the wind loads. Changes in deflections were equally small, within 0.1 mm (0.004 in.), and showed no signs of additional torsion. These results were based on the three ASCE/SEI 7-05 load cases shown in Fig. 6 only. Additionally, alternative retrofits recommended by the 2010 Florida building code for buildings with preexisting obstacles were not explored in this investigation.

Effects of Reentrant Corner Dimensions

Fig. 12 shows the lateral load distributions to the walls parallel to the wind loads and displaced shapes of the exterior wall top plates for each wind load case. For N-S design wind loads, the displaced shape of the top chords for each model variation showed little to no torsion caused by the increasing size of the reentrant corner. As Walls 7 and 9 were extended, lateral loads carried by the outer walls running N-S (Walls 5 and 9) were redistributed to the inner N-S Walls 6–8. The percent of N-S loads carried by these central walls increased by 14%, whereas the percent of N-S loads carried by the outer walls (Walls 5 and 9) decreased by 7 and 3%, respectively.

In the case of W-E wind loads, the displaced shape of the top chords clearly showed increasing degrees of torsion as the size of the reentrant corner increased. Although the relative distribution of these loads to each of the W-E walls changed by less than 5%, increasing the length of the southern end of Wall 9 (perpendicular to the wind) increased the total amount of W-E wind load on the house. As a result, the relative in-plane deflections of southern Walls 1 and 2 compared with northern Walls 3 and 4 increased dramatically. This can be attributed to the fact that Walls 1 and 2 were significantly less stiff than Walls 3 and 4 as a result of the shorter lengths and relatively large opening to surface-area ratios of Walls 1 and 2. This asymmetry in relative stiffness between the north and south sides of the house caused torsion to occur with increasing loads in the W-E direction. Wind loads applied diagonally, southeast to northwest (SE-NW), into the reentrant corner also caused increasing amounts of torsion as the size of the reentrant corner increased. For all load cases, the effects of increasing the size of the reentrant corner were dependent on the relative stiffness and location of the walls and the orientation of the wind loads. Additionally, the displaced shapes of the top plates in Fig. 12 show a combination of torsional behavior and in-plane displacements characteristic of a semirigid diaphragm.

J. Perform. Constr. Facil., 2014, 28(3): 430-439

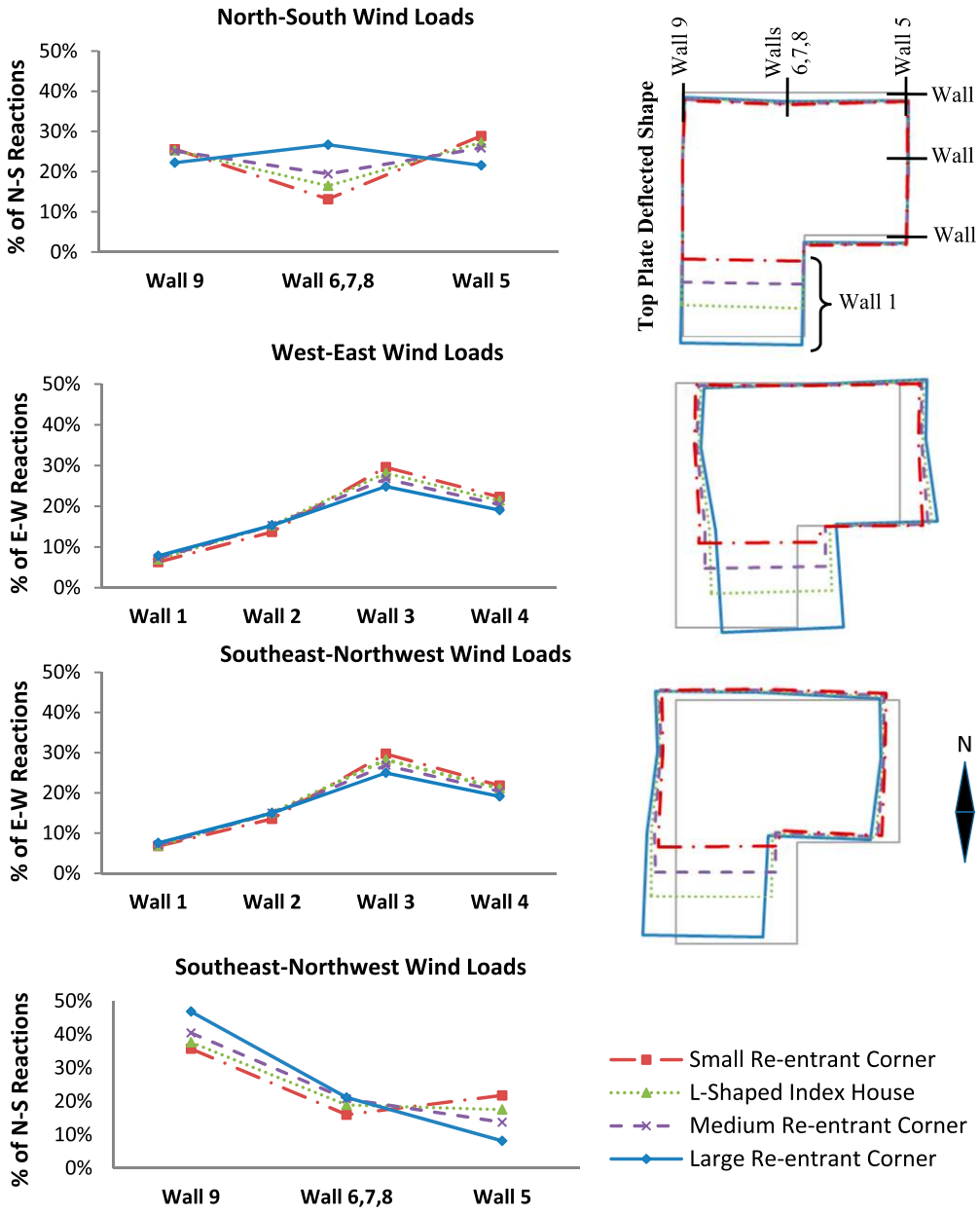

Fig. 12. Lateral load distribution and top plate deflected shapes for reentrant corner variations

The results of this study imply that balancing the stiffness of the walls along each of the major axes of the house may reduce torsion caused by large reentrant corners. In an effort to reduce torsion in the model with the largest reentrant corner, the stiffness of Walls 1 and 2 was increased by assuming realistic changes in the construction of the walls: (1) blocking was added to the walls, (2) the edge fastener spacing for the GWB was decreased to 102 mm (4 in.), (3) the nails used for the plywood were upgraded from 6d to 8d common nails, and (4) the edge nail spacing for the plywood was decreased to 51 mm (2 in.). Based on these assumptions, new values of G_{12} for the GWB and plywood sheathing on Walls 1 and 2 were calculated using the adjustment procedure described in the modeling methods section. Fig. 13 shows the deflected shapes of the original model and the model with increased stiffness in Walls 1 and 2 for the W-E and SE-NW wind loads. In both cases, increasing the stiffness of the walls on the south side of the house slightly decreased the amount of torsion seen in the deflected shape of the top chords.

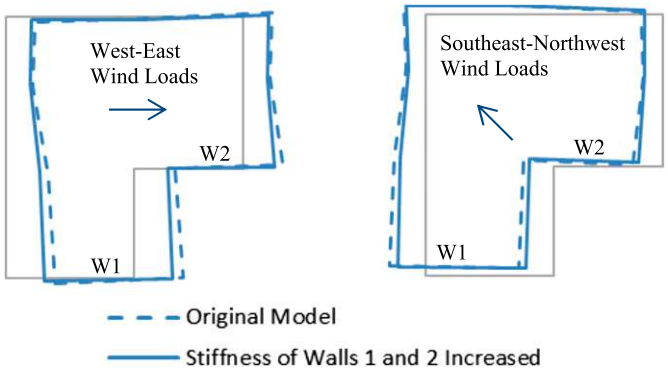

Fig. 13. Displaced shape of large reentrant corner building with increased stiffness in Walls 1 and 2

J. Perform. Constr. Facil., 2014, 28(3): 430-439

Conclusions

On the basis of validation studies, the simplified linear modeling methods created by Martin et al. (2011) and further developed in this study were capable of predicting uplift and lateral load paths in a light-frame wood residential structure with complex, realistic plan geometry. This conclusion is strictly for loading conditions within the elastic range of the structure. The modeling methods used in this study cannot be applied to inelastic or failure analysis.

Using the validated modeling methods, two different load path investigations were performed using uniform uplift pressures and ASCE/SEI 7-05 (ASCE 2005) design wind loads. The following conclusions were drawn based on results from the load path investigations:

1. The addition of a reentrant corner in a low-rise structure under uniform uplift pressure caused load concentrations at the reentrant corner and in either wall directly opposite the reentrant corner, depending on the truss orientation. For example, when the reentrant corner was extended by 2.4 m, making the dimensions of the corner a 1:1 ratio, loads carried by the internal walls parallel to the wind increased by 14%, whereas the outer walls parallel to the wind decreased by 3–7%.
2. The addition of wall openings in a low-rise structure under uniform uplift pressure caused load concentrations on either side of the openings. Uplift loads at these points of concentration were further distributed to the remaining walls by the roof trusses. The largest load concentrations occurred when an opening was placed in a side wall, directly adjacent to the reentrant corner. Openings in the walls parallel to the trusses had the least effect on uplift reactions in the remaining walls. Therefore, homes with large openings, such as garage doors in the side walls, are more vulnerable to uplift loads than ones with openings in the gable-end walls.
3. The ASCE/SEI 7-05 MWFRS (ASCE 2005) design wind loads caused uplift load concentrations at the hold-downs placed under the door jams and the corners of the L-shaped house.
4. There was no evidence that the gable-end retrofit adopted by the 2010 Florida building code caused additional torsion in the L-shaped house when loaded with ASCE/SEI 7-05 (ASCE 2005) MWFRS design wind loads.
5. The effects of increasing the size of the reentrant corner in a L-shaped house under ASCE/SEI 7-05 (ASCE 2005) MWFRS design wind loads were dependent on the location and relative stiffness of the in-plane walls and the assumed direction of the wind.

Acknowledgments

Previous research contributions from Kenneth Martin, Dr. Phillip Paevere, and Dr. Bohumil Kasal were greatly appreciated. Funding from the Oregon State University Center for Wood Utilization Research is also appreciated.

References

American Forest & Paper Association (AF&PA). (2005a). "ASD/LRFD NDS national design specification for wood construction (NDS)." *ANSI/AF&PA NDS-2005*, Washington, DC.

American Forest & Paper Association (AF&PA). (2005b). "Special design provisions for wind and seismic." *ANSI/AF&PA SDPWS-2005*, Washington, DC.

ASCE. (2005). "Minimum design loads for buildings and other structures." *ASCE/SEI 7-05*, New York.

Collins, M., Kasal, B., Paevere, P., and Foliente, G. C. (2005). "Three-dimensional model of light frame wood buildings. I: Model description." *J. Struct. Eng.*, 10.1061/(ASCE)0733-9445(2005)131:4(676), 676–683.

Computers and Structures. (2009). *CSI analysis reference manual: For SAP2000*, ETABS and SAFE, Berkeley, CA.

Dolan, J. D., and Johnson, A. C. (1996) "Monotonic tests of long shear walls with openings." *Rep. TE-1996-001*, Virginia Polytechnic Institute and State Univ. Timber Engineering, Blacksburg, VA.

Doudak, G. (2005). "Field determination and modeling of load paths in wood light-frame structures." Ph.D. thesis, McGill Univ., Montreal.

Engineered Wood Products Association of Australia. (2009). "Structural plywood and LVL design manual." *EWPAA design guides*, ⟨http://www.ed.ewp.asn.au/Public_Access/Library/library_search.aspx?criteria=design&type=All⟩ (Jul. 19, 2012).

Gypsum Association. (2010). "Gypsum board typical mechanical and physical properties." *GA 235-10*, Gypsum Association, Hyattsville, MD.

Holmes, J. D. (2001). *Wind loading of structures*, Spon Press, New York.

International Code Council (ICC). (2011). *Florida building code 2010—Residential*, Country Club Hills, IL.

Kasal, B. (1992). "A nonlinear three-dimensional finite-element model of a light-frame wood structure." Ph.D. thesis, Oregon State Univ., Corvallis, OR.

Martin, K. G., Gupta, R., Prevatt, D. O., Datin, P. L., and van de Lindt, J. W. (2011). "Modeling system effects and structural load paths in a wood-framed structure." *J. Archit. Eng.*, 10.1061/(ASCE)AE.1943-5568.0000045, 134–143.

Mehta, K. C., and Coulbourne, W. L. (2010). *Wind loads: Guide to the wind load provisions of ASCE 7-05*, ASCE, Reston, VA.

Nairn, J. (2007). "OSULaminates." ⟨http://www.cof.orst.edu/cof/wse/faculty/Nairn/OSULaminates.html⟩ (Jul. 31, 2012).

Paevere, P. (2002). "Full-scale testing, modeling and analysis of light-frame structures under lateral loading." Ph.D. thesis, Univ. of Melbourne, Parkville, VIC, Australia.

Paevere, P. J., Foliente, G. C., and Kasal, B. (2003). "Load-sharing and redistribution in a one-story woodframe building." *J. Struct. Eng.*, 10.1061/(ASCE)0733-9445(2003)129:9(1275), 1275–1284.

Patton-Mallory, M., Gutkowski, R. M., and Solstis, L. A. (1984). "Racking performance of light-frame walls sheathed on two sides." *FPL-448*, Forest Products Laboratory, Madison, WI.

Pfretzschner, K. S. (2012). "Practical modeling for load paths in a realistic, light-frame wood house." M.S. thesis, Oregon State Univ., Corvallis, OR.

Phillips, T. L., Itani, R. Y., and McLean, D. I. (1993). "Lateral load sharing by diaphragms in wood-framed buildings." *J. Struct. Eng.*, 10.1061/(ASCE)0733-9445(1993)119:5(1556), 1556–1571.

Prevatt, D. O., et al. (2012). "Building damage observations and EF classifications from the Tuscaloosa, AL and Joplin, MO tornadoes." *Structures Congress 2012*, ASCE, Reston, VA, 999–1010.

Seaders, P. (2004). "Performance of partially and fully anchored wood frame shear walls under monotonic, cyclic and earthquake loads." M.S. thesis, Oregon State Univ., Corvallis, OR.

Shivarudrappa, R., and Nielson, B. G. (2011) "Sensitivity of load distribution in light-framed wood roof systems due to typical modeling parameters." *J. Perform. Constr. Facil.*, 10.1061/(ASCE)CF.1943-5509.0000323, 222–234.

Simpson Strong-Tie. (2014). "HDB/HD holdowns." ⟨http://www.strongtie.com/products/connectors/HDB-HD.asp#⟩ (Mar. 12, 2014).

Suksawang, N., and Mirmiran, A. (2009). "Hurricane loss reduction for housing in Florida: Performance of gable end wall bracing retrofit for hurricane protection, phase II." ⟨http://www.ihrc.fiu.edu/wp-content/uploads/2012/05/HLMP_Year09_Section4_GableEndBracing_RCMP08-09.pdf⟩ (Jul. 22, 2012).

van de Lindt, J. W., et al. (2007). "Performance of wood-frame structures during Hurricane Katrina." *J. Perform. Constr. Facil.*, 10.1061/(ASCE)0887-3828(2007)21:2(108), 108–116.

Wolfe, R. W., and McCarthy, M. (1989). "Structural performance of light frame roof assemblies—I. Truss assemblies with high truss stiffness variability." *FPL-RP-492*, Forest Products Laboratory, Madison, WI.

Wolfe, R. W., Percival, D. H., and Moody, R. C. (1986). "Strength and stiffness of light framed sloped trusses." *FPL-RP-471*, Forest Products Laboratory, Madison, WI.

J. Perform. Constr. Facil., 2014, 28(3): 430-439